arXiv:0810.0813v2 [astro-ph] 30 Nov 2008

Modeling Nonlinear Evolution of Baryon Acoustic Oscillations: Convergence Regime of *N*-body Simulations and Analytic Models

Takahiro Nishimichi[1], Akihito Shirata[1,2], Atsushi Taruya[1,3,5], Kazuhiro Yahata[1], Shun Saito[1], Yasushi Suto[1,3], Ryuichi Takahashi[4], Naoki Yoshida[4,5], Takahiko Matsubara[4], Naoshi Sugiyama[4,5], Issha Kayo[4,5], Yipeng Jing[6], and, Kohji Yoshikawa[7]

[1]*Department of Physics, School of Science, The University of Tokyo, Tokyo 113-0033*

[2]*Department of Physics, Tokyo Institute of Technology, Tokyo 152-8511*

[3]*Research Center for the Early Universe, The University of Tokyo, Tokyo 113-0033*

[4]*Department of Physics and Astrophysics, Nagoya University, Chikusa, Nagoya 464-8602*

[5]*Institute of Physics and Mathematics of the Universe, The University of Tokyo, 5-1-5 Kashiwa-no-ha, Kashiwa City, Chiba 277-8582*

[6] *Shanghai Astronomical Observatory, Nandan Road 80, Shanghai 200030, China*

[7]*Centre for Computational Sciences, University of Tsukuba, Tsukuba 305-8577*

nishimichi@utap.phys.s.u-tokyo.ac.jp

(Received 0 0; accepted 0 0)

Abstract

We use a series of cosmological N-body simulations and various analytic models to study the evolution of the matter power spectrum in real space in a Λ Cold Dark Matter universe. We compare the results of N-body simulations against three analytical model predictions; standard perturbation theory, renormalized perturbation theory, and the closure approximation. We include the effects from finite simulation box size in the comparison. We determine the values of the maximum wavenumbers, $k_{1\%}^{\rm lim}$ and $k_{3\%}^{\rm lim}$, below which the analytic models and the simulation results agree to within 1 and 3 percent, respectively. We then provide a simple empirical function which describes the convergence regime determined by comparison between our simulations and the analytical models. We find that if we use the Fourier modes within the convergence regime alone, the characteristic scale of baryon acoustic oscillations can be determined within 1% accuracy from future surveys with a volume of a few $h^{-3}{\rm Gpc}^3$ at $z\sim1$ or $z\sim3$ in the absence of any systematic distortion of the power spectrum.

Key words: cosmology: large-scale structure of universe — methods: statistical

1. Introduction

The nature of dark energy remains one of the most fundamental questions in physics and cosmology. It is accessible only through astronomical observations, and a number of large galaxy redshift surveys and weak-lensing observations are expected to yield tight constraints on the dark energy equation of state parameter, $w_{\rm DE} \equiv p_{\rm DE}/\rho_{\rm DE}$. The use of baryon acoustic oscillations (hereafter BAOs) is a promising tool to determine $w_{\rm DE}$. The characteristic scale of BAOs can be used as a robust standard ruler, which helps us to reconstruct the expansion history of the universe.

Substantial improvements in theories as well as observations are required to constrain $w_{\rm DE}$ within an accuracy of a few percent, which is the goal of next generation BAO surveys. Nishimichi et al. (2007) showed that the measurements of the angular diameter distance and of the Hubble parameter must be very accurate, with errors less than 1%, in order to constrain $w_{\rm DE}$ at a 5% level at $z \sim 1$ in the special case that the other cosmological parameters are fixed. Clearly, theoretical models are required to predict the matter power spectrum with even better accuracy.

Recently, significant progress has been made in developing analytic models of the matter power spectrum by extending conventional perturbation theory (e.g., Crocce & Scoccimarro 2006a, b, 2008; Matarresse & Pietroni 2007, 2008; Valageas 2007; Taruya & Hiramatsu 2008; Matsubara 2008). Cosmological N-body simulations are often used as a reference to calibrate these models. It is not clear, however, whether or not N-body simulations provide sufficiently accurate results at the required percent level even at weakly nonlinear scales where perturbation theory is generally supposed to be reasonably accurate.

Indeed a variety of systematic effects needs to be considered in interpreting the results of N-body simulations. It is well known that discreteness of a density field in N-body simulations causes spurious behaviour of the power spectrum at length scales comparable to or smaller than the mean inter-particle separation (Melott et al. 1997; Splinter et al. 1998; Hamana, Yoshida & Suto 2002; Baertschiger, Joyce & Sylos Labini 2002; Marcos et al. 2006; Joyce & Marcos 2007a, b; Joyce, Marcos & Baertschiger 2008; Romeo et al. 2008). Adopting a finite-size simulation box and imposing a periodic boundary condition also systematically biases the growth of density fluctuations at almost all the length scales (Seto 1999). Recently, Takahashi et al. (2008) examined the effect of the finite number of Fourier modes in a *single* N-body realization due to a finite box size. They found that the evolution of the power spectrum measured from each realization deviates from the prediction of perturbation theory by more than a few percent even at very large scales (e.g. $k \lesssim 0.1h{\rm Mpc}^{-1}$) and that this deviation results from having only a finite number of modes, which can be explained by including second-order perturbation contributions. This implies that a sub-percent level accuracy both in theories and in simulations is very demanding and we need to explore this in detail.

In the present paper, we consider a specialized case of the matter power spectrum in real space. We critically compare the evolution of the matter density fluctuations in the weakly nonlinear regime in cosmological simulations to that of theoretical predictions. We measure the matter power spectra using the simulation outputs and compare them with analytic models. In doing so we correct for the finite-mode effect pointed out by Takahashi et al. (2008). Unlike the conventional approach, we do not regard the results of N-body simulations as perfect calibrators of analytical models. We determine ranges of wavenumbers where both theories and N-body simulations agree within a given accuracy.

The rest of the present paper is organized as follows. Section 2 briefly outlines the analytic models that we examine for the nonlinear matter power spectrum. Section 3 describes our simulation details. Our methods to measure the matter power spectrum and to correct for the finite volume effect are shown in section 4. We show our results of N-body simulations and determine the convergence regime in wavenumber in section 5. We also discuss the phase information of BAOs and predict the parameter forecast from the modes in this convergence regime alone in section 6. Finally section 7 summarizes the present paper. The convergence tests of our N-body simulations are discussed in the appendix.

2. Analytic Nonlinear Models

Various analytic models have been proposed to account for nonlinear evolution of the matter power spectra in real space. In this paper, we will compare N-body simulations with three different analytic models, specifically focusing on the leading-order contributions. The models include standard perturbation theory (SPT; e.g., Bernardeau et al. 2002), renormalized perturbation theory (RPT; Crocce & Scoccimarro 2006a, b, 2008), and the closure approximation (CLA; Taruya & Hiramatsu 2008).

SPT is a straightforward expansion of the fluid equations around their linear solution, assuming that fluctuation amplitudes are small. Schematically, the expansion is written

$$P(k,z) = P^{\rm L}(k,z) + P^{\rm 1-loop}(k,z) + \cdots, \tag{1}$$

where $P^{\rm L}(k,z)$ is the linear power spectrum, which grows as $\propto D_+^2(z)$ with linear growth rate, $D_+(z)$. The second term, $P^{\rm 1-loop}(k,z)$, is the one-loop correction to the power spectrum, which represents the contributions coming from the second-order and third-order solutions. The one-loop correction is roughly proportional to $P^{\rm L}\Delta_0^2$ with $\Delta_0^2 = k^3P^{\rm L}(k,z)/(2\pi^2)$, and this term subsequently exceeds the linear term at lower redshift and smaller scales. The explicit expressions for the one-loop correction $P^{\rm 1-loop}(k,z)$ may be found in the literature (e.g., Makino, Sasaki & Suto 1992; Jain & Bertschinger 1994; Scoccimarro & Frieman 1996; Jeong & Komatsu 2006; Nishimichi et al. 2007).

Both RPT and CLA are constructed from the renormalized expression of a perturbation series obtained from SPT, by introducing non-perturbative statistical quantities such as

the propagator and the vertex function. The resultant *renormalized* expressions for the power spectrum are given as an infinite series of irreducible diagrams composed of the propagator, the vertex function, and the power spectra themselves in a fully non-perturbative way. Then, employing the Born approximation, RPT of Crocce & Scoccimarro (2008) perturbatively evaluates the renormalized diagrams under the tree-level approximation of vertex functions. In contrast, CLA proposed by Taruya & Hiramatsu (2008) first truncates the renormalized expansion at the one-loop order under the tree-level approximation of vertex functions, and obtains a closed set of equations for the power spectrum and the propagator. In practice, they further apply the Born approximation to the truncated diagram. As a result, the leading-order calculations of the power spectra in CLA reduce to the same analytic expression as in the case of RPT, leading to

$$P(k,z) = G^2(k,z)P^{\rm L}(k,z_{\rm ini}) + P_{\rm MC}^{\rm 1-loop}(k,z) + \cdots. \tag{2}$$

Here, the function $G(k,z)$ is the propagator, and the term $P_{\rm MC}^{\rm 1-loop}(k,z)$ represents the corrections generated by mode-mode coupling at smaller scales, constructed from the one-loop diagram. In the above expression, the only difference between CLA and RPT is the asymptotic behavior of the propagator. The explicit expressions for the propagator together with the mode-coupling term are summarized in Crocce & Scoccimarro (2006b, 2008) and Taruya & Hiramatsu (2008).

We note here that the most important difference between SPT and RPT/CLA is the convergence properties dictated by the propagator. Similar to $P^{\rm 1-loop}(k,z)$ of SPT, the term $P_{\rm MC}^{\rm 1-loop}(k,z)$ is roughly proportional to $P^{\rm L}\Delta_0^2$, but it additionally contains propagators, leading to a large suppression at high k. Therefore, to the one-loop level, RPT and CLA are expected to be most accurate at low k (below the propagator damping scale), but the predictions at low k are expected to be much accurate for RPT/CLA compared to SPT.

3. Simulations

In this section we describe our fiducial simulations. We also run some simulations with different settings (initial conditions, integrators and box sizes), which are discussed in the appendix.

We begin with an explanation of our initial conditions for the N-body simulations. We compute the linear power spectrum at an initial redshift $z_{\rm ini} = 31$ using `CAMB` (Lewis, Challinor & Lasenby 2000). For all the simulations in the present paper, we adopt the standard ΛCDM model with the cosmological parameters from the WMAP3 results (Spergel et al. 2007), $\Omega_m = 0.234$, $\Omega_\Lambda = 0.766$, $\Omega_b = 0.0414$, $h = 0.734$, $\sigma_8 = 0.76$ and $n_s = 0.961$, which are the current matter, cosmological constant, baryon densities in units of the critical density, the Hubble constant in units of $100{\rm km\,s^{-1}Mpc^{-1}}$, density fluctuation amplitude smoothed with a top-hat filter of radius $8h^{-1}$Mpc, and the scalar spectral index, respectively (see table 1). We then generate a linear overdensity field in Fourier space assuming Gaussianity; the amplitude follows

Table 1. Adopted cosmological and simulation parameters of `Gadget-2` for our fiducial runs.

cosmological	Ω_m	Ω_Λ	Ω_b/Ω_m	h	σ_8	n_s
value	0.234	0.766	0.175	0.734	0.76	0.961
simulation	box size	# of particles	$z_{\rm ini}$	# of PM grids	softening length	$N^{\rm run}$
value	$1000h^{-1}$Mpc	512^3	31	1024^3	$0.1h^{-1}$Mpc	4

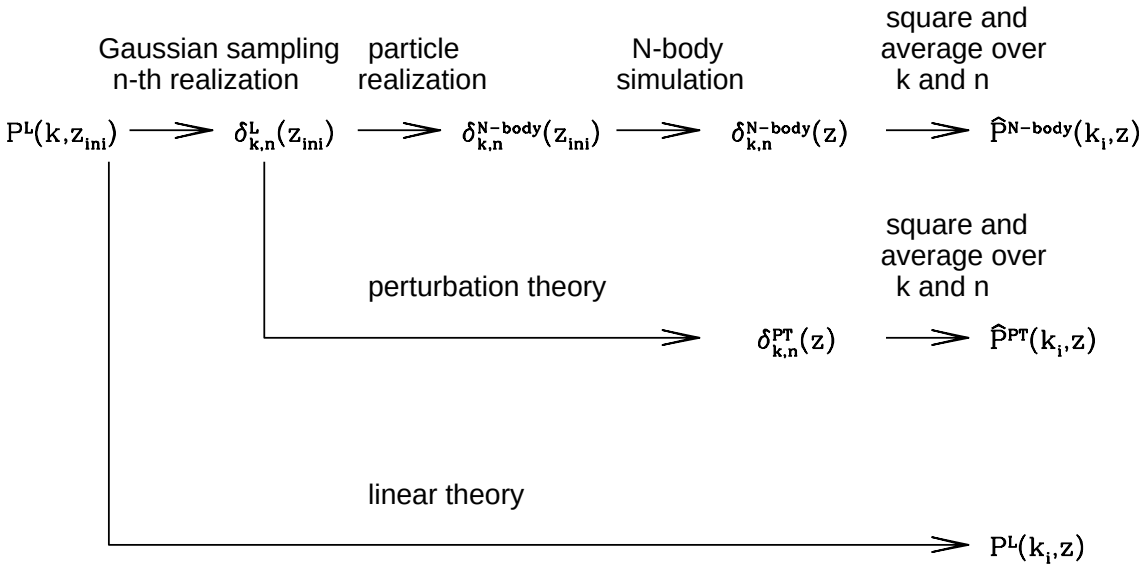

Fig. 1. A flow chart to illustrate our methodology to correct for the effect of finite box size.

the Rayleigh distribution, and the phase is uniformly distributed. We employ 512^3 dark matter particles within a cube of $1000h^{-1}$Mpc in each side. We displace these particles from regular grid pre-initial positions using the second-order Lagrangian perturbation theory (2LPT; e.g., Crocce, Pueblas & Scoccimarro 2006).

We next describe the time integration scheme. We adopt a publicly available parallel cosmological N-body solver `Gadget2` (Springel 2005). The number of meshes used in the particle-mesh computation is 1024^3. We adopt a softening length of $0.1h^{-1}$Mpc for the tree forces. We select three output redshifts; $z = 3$, 1 and 0, where we measure the power spectrum (see section 4 for more details).

In the appendix, we discuss the convergence of our simulations against different initial conditions, box sizes, and codes. We found that the current setup provides a convergent result within 1% of the amplitude of the power spectrum at our scales of interest ($k \lesssim 0.4h{\rm Mpc}^{-1}$). We use this setup as our fiducial model, and run 4 different realizations for this model.

Table 2. Notations for various density contrasts and power spectra.

	meaning	description
$P^{\rm L}(k,z)$	input linear power spectrum	text in §2
$\delta^{\rm L}_{\mathbf{k},n}(z)$	density contrast Gaussian-sampled from $P^{\rm L}(k,z)$ for the n-th realization	text in §3
$\delta^{N-{\rm body}}_{\mathbf{k},n}(z)$	density contrast realized by particles using 2LPT displacement and evolved by N-body simulation	text in §3
$\hat{P}^{N-{\rm body}}(k_i,z)$	power spectrum of the i-th wavenumber bin estimated from N-body simulations taking average over finite modes and realizations	Eq.(3)
$\delta^{\rm PT}_{\mathbf{k},n}(z)$	$\delta^{\rm L}_{\mathbf{k},n}(z)$ evolved by perturbation theory	Eq.(11)
$\hat{P}^{\rm PT}(k_i,z)$	same as $\hat{P}^{N-{\rm body}}(k_i,z)$ but calculated from $\delta^{\rm PT}_{\mathbf{k},n}(z)$, not $\delta^{N-{\rm body}}_{\mathbf{k},n}(z)$	Eq.(10)
$\hat{P}^{N-{\rm body}}_{\rm corrected}(k_i,z)$	$\hat{P}^{N-{\rm body}}(k,z)$ corrected for the effect of finite volume	Eq.(12)

4. Power Spectrum Analysis

4.1. Matter density field and power spectrum in N-body simulations

Here we briefly describe the notation for various density fields and power spectra which we use throughout the paper (see figure 1 and table 2).

We denote the Gaussian-sampled density field from $P^{\rm L}(k,z_{\rm ini})$ by $\delta^{\rm L}_{\mathbf{k},n}(z_{\rm ini})$, where the subscript n stands for the n-th realization. We then denote by $\delta^{N-{\rm body}}_{\mathbf{k},n}(z_{\rm ini})$ the density field *realized* by particles using 2LPT displacement. Note that $\delta^{\rm L}_{\mathbf{k},n}(z_{\rm ini})$ is different from $\delta^{N-{\rm body}}_{\mathbf{k},n}(z_{\rm ini})$; the former is strictly Gaussian, whereas the latter slightly deviates from Gaussian because of the nonlinearity and discreteness in the process of displacement. The measured density contrast from the simulation output at redshift z is also expressed as $\delta^{N-{\rm body}}_{\mathbf{k},n}(z)$. In measuring $\delta^{N-{\rm body}}_{\mathbf{k},n}(z)$ from the simulation output, we first assign particles onto a 1024^3 mesh using Cloud-in-Cells interpolation (Hockney & Eastwood 1981). We then use a FFT to calculate density contrasts in Fourier space, and divide each Fourier mode by the Fourier transform of the window function (Angulo et al. 2008). We made sure that the details of the interpolation scheme and the number of mesh points do not affect the results significantly in the scales of our interest ($k \lesssim 0.4h$ Mpc $^{-1}$). See also Jing (2005) for a discussion of the effects of aliasing.

We square $\left|\delta^{N-{\rm body}}_{{\rm k},n}(z)\right|$ and take an average over realizations and modes:

$$\hat{P}^{N-{\rm body}}(k_i,z) \equiv \left\langle \left|\delta^{N-{\rm body}}_{\mathbf{k},n}(z)\right|^2 \right\rangle_i \equiv \frac{1}{N^{\rm mode}_i N^{\rm run}} \sum_{k^{\rm min}_i<|\mathbf{k}|<k^{\rm max}_i} \sum_{n=1}^{N^{\rm run}} \left|\delta^{N-{\rm body}}_{\mathbf{k},n}(z)\right|^2, \quad (3)$$

$$k_i \equiv \frac{1}{N^{\rm mode}_i} \sum_{k^{\rm min}_i<|\mathbf{k}|<k^{\rm max}_i} |\mathbf{k}|\,, \quad (4)$$

where $N^{\rm mode}_i$ and $N^{\rm run}$ are the numbers of modes in the i-th wavenumber bin and the number of

realizations, and $k_i^{\rm min}$ and $k_i^{\rm max}$ are the minimum and the maximum wavenumber, respectively. Note that we use $\langle ... \rangle_i$ to denote the average over modes in the i-th wavenumber bin and over realizations: this average is not equivalent to the true ensemble average, and the difference corresponds to the finiteness of the simulated volume (or number of modes). In what follows, we adopt equally-spaced bins with width $\Delta k = 0.005h{\rm Mpc}^{-1}$.

Finally, the standard errors of the averaged power spectra of equation (3) can be estimated by

$$\left[\text{error of } \hat{P}^{N-\rm body}(k_i,z)\right]^2 = \frac{\left\langle \left[\left|\delta^{N-\rm body}_{\mathbf{k},n}(z)\right|^2 - \hat{P}^{N-\rm body}(k_i,z) \right]^2 \right\rangle_i}{N_i^{\rm mode} N^{\rm run}}. \tag{5}$$

Note that this value indicates the uncertainty in the estimation of the central value, not the variance among the modes in each bin.

4.2. Corrections to the power spectrum

The matter power spectrum measured from simulations deviates from the prediction for the ideal ensemble average, which can be obtained only in the limit of an infinite number of realizations or an infinite box size. This deviation is actually important in interpreting the results of N-body simulations as shown by Takahashi et al. (2008); the matter power spectrum measured from their N-body simulations does not agree with the predictions of linear theory nor SPT even at very large scales (e.g., $k \lesssim 0.1h{\rm Mpc}^{-1}$). They examined the effect of a finite box size (hence a finite number of modes) and showed that the finite-mode effect is actually responsible for the anomalous growth rate. Here we briefly summarize their formulation of the correction.

We follow the standard notation used in cosmological perturbation theory [see Bernardeau et al. (2002) for a review]. Let us expand the density perturbations in k-space for the n-th N-body realization as

$$\delta^{N-\rm body}_{\mathbf{k},n}(z) = \delta^{\rm L}_{\mathbf{k},n}(z) + \delta^{(2)}_{\mathbf{k},n}(z) + ... \tag{6}$$

Here the second-order term is expressed as a sum of contributions from mode couplings between two modes:

$$\delta^{(2)}_{\mathbf{k},n}(z) = \sum_{\mathbf{p}} F^{(2)}(\mathbf{p}, \mathbf{k}-\mathbf{p}; z) \delta^{\rm L}_{\mathbf{p},n}(z) \delta^{\rm L}_{\mathbf{k}-\mathbf{p},n}(z), \tag{7}$$

where the symmetrized second-order kernel $F^{(2)}$ is expressed as

$$F^{(2)}(\mathbf{x},\mathbf{y};z) = \frac{1}{2}\left[1+\epsilon(z)\right] + \frac{1}{2}\frac{\mathbf{x}\cdot\mathbf{y}}{xy}\left(\frac{x}{y}+\frac{y}{x}\right) + \frac{1}{2}\left[1-\epsilon(z)\right]\frac{(\mathbf{x}\cdot\mathbf{y})^2}{x^2y^2}, \tag{8}$$

$$\epsilon(z) \approx \frac{3}{7}\Omega_m^{-1/143}(z). \tag{9}$$

In practice, the time dependence of the kernel function is very weak, and thus we simply set $\epsilon = 3/7$ in what follows. The power spectrum up to the third order in $\delta^{\rm L}_{\mathbf{k},n}(z)$ averaged over

modes in the i-th wavenumber bin and over realizations is

$$\hat{P}^{\rm PT}(k_i,z) \equiv \left\langle \left|\delta^{\rm PT}_{\mathbf{k},n}\right|^2 \right\rangle_i , \tag{10}$$

$$\left|\delta^{\rm PT}_{\mathbf{k},n}\right|^2 \equiv \left|\delta^{\rm L}_{\mathbf{k},n}(z)\right|^2 + 2\Re\left[\delta^{\rm L}_{\mathbf{k},n}(z)\delta^{(2)}_{-\mathbf{k},n}(z)\right], \tag{11}$$

where $\Re[...]$ stands for the real part of a complex number. Though the second term should vanish for an ensemble average over infinite modes, it does not vanish exactly if the number of Fourier modes is finite. The first term grows as $\propto D_+^2(z)$ while the second term grows as $\propto D_+^3(z)$, thus the second term becomes important at late time (i.e., at low redshifts).

The method to correct for the deviation from the ideal ensemble average is to multiply $\hat{P}^{N-\rm body}(k_i,z)$ by the ratio of $\hat{P}^{\rm PT}(k_i,z)$ and $P^{\rm L}(k_i,z)$:

$$\hat{P}^{\rm N-body}_{\rm corrected}(k_i,z) \equiv \hat{P}^{\rm N-body}(k_i,z) \times P^{\rm L}(k_i,z)/\hat{P}^{\rm PT}(k_i,z). \tag{12}$$

The individual random nature of each N-body run in both $\hat{P}^{\rm N-body}(k_i,z)$ and $\hat{P}^{\rm PT}(k_i,z)$ is weakened by this procedure [equation (12)] as long as the predictions of perturbation theory are sufficiently accurate. This method does not bias the corrected value of the power spectrum even if the perturbation theory breaks down, since $\hat{P}^{\rm PT}(k_i,z)$ approaches $P^{\rm L}(k_i,z)$ in the limit of infinite number of Fourier modes.

As in equation (5), the standard errors of equation (12) can be estimated as

$$\left[\text{error of } \hat{P}^{N-\rm body}_{\rm corrected}(k_i,z)\right]^2 = \frac{\left\langle \left[\left|\delta^{N-\rm body}_{\mathbf{k},n}(z)\right|^2 - \frac{\hat{P}^{N-\rm body}(k_i,z)}{\hat{P}^{\rm PT}(k_i,z)} \left|\delta^{\rm PT}_{\mathbf{k},n}(z)\right|^2 \right]^2 \right\rangle_i}{N^{\rm run} N^{\rm mode}_i}. \tag{13}$$

The average of $\left|\delta^{N-\rm body}_{\mathbf{k},n}(z)\right|^2$ is $\hat{P}^{N-\rm body}(k_i,z)$ while that of $\left|\delta^{\rm PT}_{\mathbf{k},n}(z)\right|^2$ is $\hat{P}^{\rm PT}(k_i,z)$, and thus we multiply the ratio in the second term in the numerator to adjust the mean values.

5. Results

5.1. Comparison between N-body simulations and analytic models

As mentioned before, the accuracy of N-body simulations themselves is not perfect and we do not regard them as perfect calibrators of theoretical models. Instead we compare the power spectrum of our simulations with those from theoretical predictions aiming at determining the reliable range of wavenumbers in which both simulations and theoretical models agree.

We first compare the averaged power spectrum over the four realizations without any corrections to the theoretical predictions. The left panel of figure 2 plots the fractional differences from the linear power spectrum, $P^{\rm nw}(k,z)$, computed from no-wiggle formula of Eisenstein & Hu (1998). The errorbars indicate the standard errors of the estimated mean value [equation (5)]. To clarify the differences between the N-body results and theoretical predictions, we also plot the residuals from RPT in the right panel of figure 2.

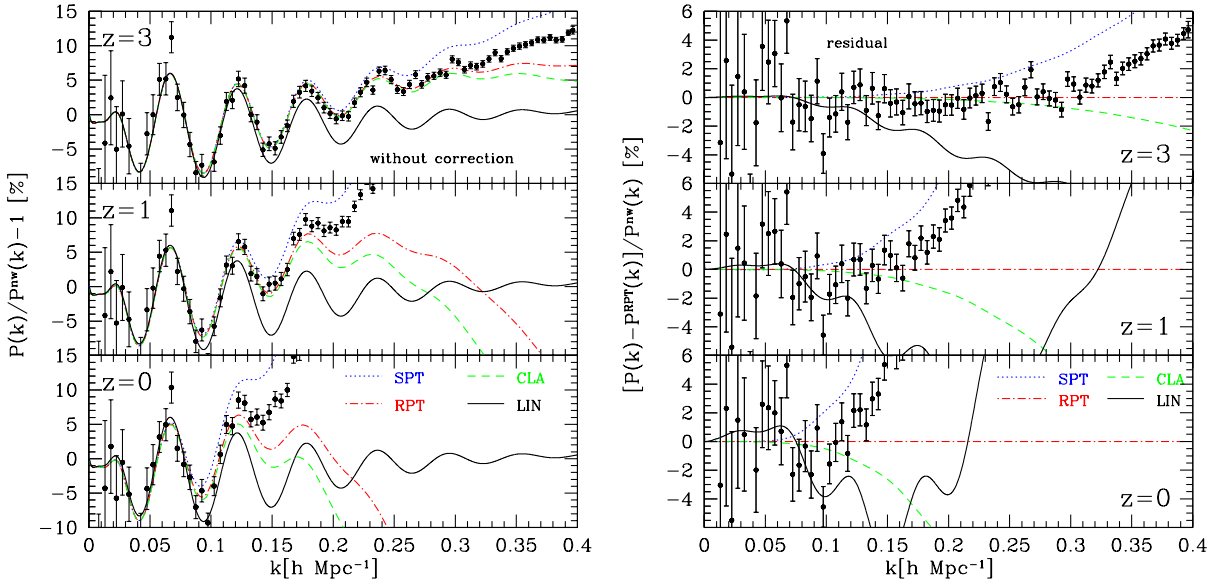

Fig. 2. Comparison of simulation power spectra and analytical predictions: *Left*: Power spectra of our simulations before correction, normalized by the no-wiggles formula; *top* $z = 3$, *middle* $z = 1$, *bottom* $z = 0$. The errorbars show the standard errors [equation (5)]. Lines are theoretical predictions described in section 2; *dotted*: standard perturbation theory (SPT), *dot-dashed*: renormalized perturbation theory (RPT), *dashed*: closure approximation (CLA), *solid*: linear theory (LIN). *Right*: Same as the left panel but we plot the difference from the RPT prediction.

Since large errorbars at $k \lesssim 0.1h\mathrm{Mpc}^{-1}$ are expected to come mostly from the finite volume effect, we next correct for this. In figure 3, we plot the power spectra, based on the procedure in § 4.2, but we truncate the expansion of equation (11) at the first term (*left*: the fractional difference from the no-wiggles formula, *right*: residuals from RPT prediction). The errorbars become significantly smaller compared with those in figure 2, because the finiteness effect is reduced by our methodology. Nevertheless, the results of N-body simulation still exhibit a few percent error, even after the correction.

Next we include the second term of equation (11) for the correction, which is coming from the mode couplings among finite modes. Figure 4 shows the results for both the fractional difference from the no-wiggles formula (left), and the residuals from RPT predictions (right). Now the size of errorbars are further reduced to the sub-percent level.

All the theoretical predictions plotted in figure 4 and N-body simulations agree with each other well within the errorbars at large scales up to some wavenumbers (we will determine the range of convergence in the next subsection). Among the four theoretical predictions, linear theory deviates from the rest at the smallest wavenumber. The range of agreement is wider for SPT than linear theory, as SPT includes the leading-order contribution of nonlinear growth. RPT and CLA seem to show better agreement with N-body simulations compared with SPT although all of the three nonlinear models include their own leading-order nonlinear corrections.

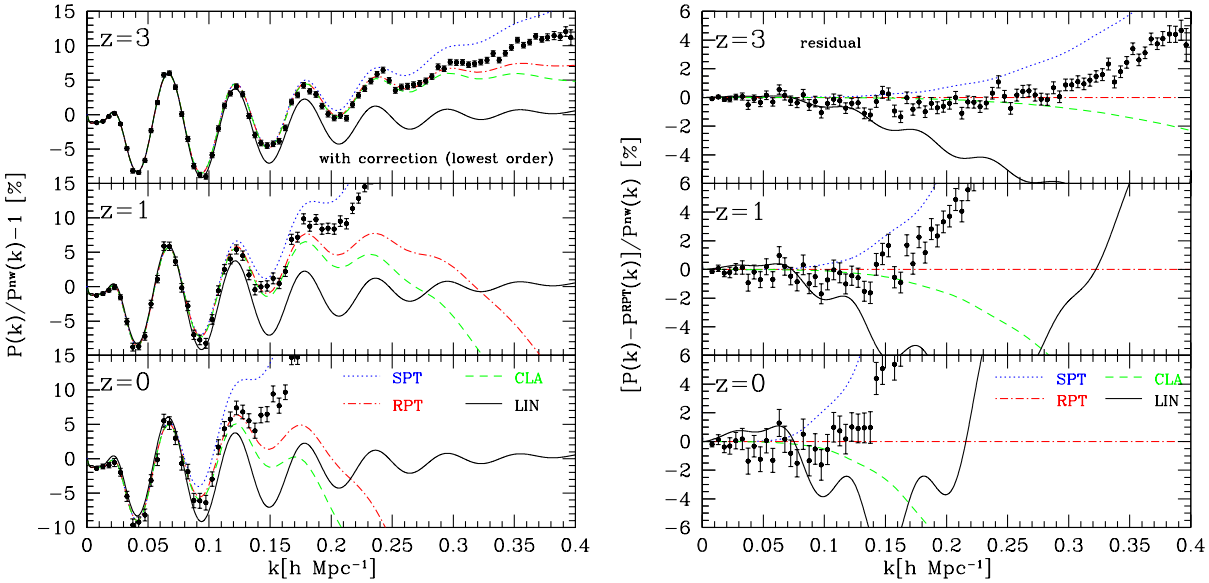

Fig. 3. Same as figure 2, but we correct for the effect of finite volume. We truncate the expansion of equation (11) at the first term. The errorbars show equation (13).

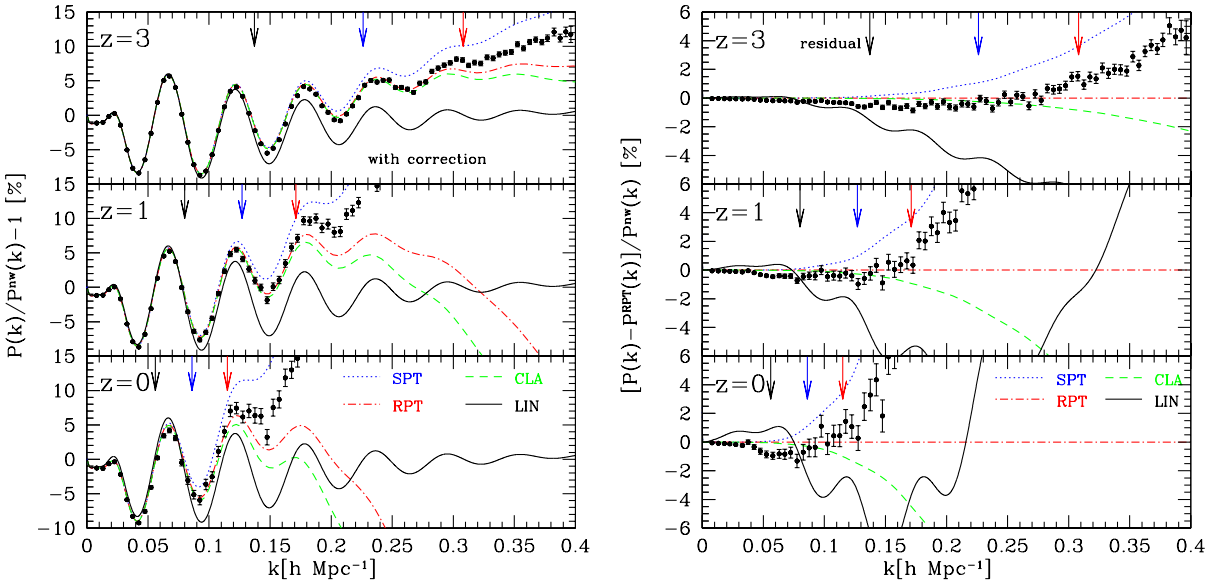

Fig. 4. Same as figure 2, but we correct for the effect of finite volume including the second term of equation (11). We also show the 1% limit wavenumbers, $k_{1\%}^{\rm lim}$, for LIN, SPT and RPT/CLA by vertical arrows (from left to right).

This difference in the agreement ranges corresponds to their different convergence properties; RPT and CLA show better convergence at scales where nonlinearity is very weak.

5.2. *Convergence regime in wavenumber*

We are now able to quantitatively estimate the convergence regime of wavenumber where theories and N-body simulations agree. We define two characteristic wavenumbers, $k_{1\%}^{\rm lim}$ and $k_{3\%}^{\rm lim}$, such that the results of N-body simulations and theoretical prediction agree within 1% at $k < k_{1\%}^{\rm lim}$ and within 3% at $k < k_{3\%}^{\rm lim}$, respectively. We confirmed that if we add 1% (3%) Gaussian errors on the power spectra binned by $\Delta k = 0.005h{\rm Mpc}^{-1}$ that leads to a $\sim 2\%$ ($\sim 6\%$) error on the dark energy equation of state parameter $w_{\rm DE}$ at $z = 1$ using the phase information of BAOs, which is roughly the goal of upcoming (ongoing) surveys.

Before determining the wavenumbers, we briefly summarize three convergence criteria previously introduced in the literature. The first one is

$$\Delta^2(k,z) \equiv \frac{k^3 P^{\rm SPT}(k,z)}{2\pi^2} < 0.4, \tag{14}$$

introduced by Jeong & Komatsu (2006) as a 1% convergence regime of SPT. The second one is introduced by Sefusatti & Komatsu (2007):

$$\sigma^2(R_{\rm min},z) \equiv \int d^3k \tilde{W}^2(qR_{\rm min}) P^{\rm L}(q,z) = 0.25, \tag{15}$$

$$k_{\rm max} = \frac{\pi}{2R_{\rm min}}, \tag{16}$$

where $\tilde{W}(qR_{\rm min})$ denotes the Fourier transform of a top-hat window function with radius $R_{\rm min}$. The third one is proposed by Matsubara (2008):

$$k^2\sigma_v^2 \equiv \frac{k^2}{6\pi^2}\int_0^\infty P^{\rm L}(q,z)dq < 0.25, \tag{17}$$

where σ_v^2 is the one-dimensional linear velocity dispersion. This gives a scale where nonlinearity becomes important. Note that Crocce & Scoccimarro (2006) presented similar criteria.

We show these criteria by dotted lines against redshift in figure 5. The dotted curve labeled with "JK06" represents the $k_{1\%}^{\rm lim}$ determined from equation (14), and the $k_{\rm max}$ of equation (16) is shown by "SK07", and the nonlinear scale of equation (17) is shown by "M08". Among these three criteria, the first two have similar redshift dependence. This is because they are based on a *local* value of the power spectrum or its Fourier transform convolved with a window function. The other criterion of Matsubara (2008) refers to the integrated value of the power spectrum over scale and thus this shows a rather mild redshift dependence of the maximum wavenumber.

The values of $k_{1\%}^{\rm lim}$ and $k_{3\%}^{\rm lim}$ can be directly read off from figure 4, which are shown in table 3 and also in figure 5 ($k_{1\%}^{\rm lim}$ by filled symbols and $k_{3\%}^{\rm lim}$ by open symbols. *squares*: RPT/CLA, *triangles*: SPT, *circles*: LIN). We empirically find that a modified version of equation (17):

$$\frac{k^2}{6\pi^2}\int_0^k P^{\rm L}(q,z)dq < C, \tag{18}$$

well reproduces the results in a unified fashion. The constant C in the right-hand-side depends on the choice of theoretical model and the threshold value (1% or 3% in this paper). We find

Table 3. The values of $k^{\rm lim}_{1\%}$ and $k^{\rm lim}_{3\%}$ read from figure 4 and the corresponding constant value in equation (18).

	$k^{\rm lim}_{1\%}$ [hMpc^{-1}]			$C_{1\%}$	$k^{\rm lim}_{3\%}$ [hMpc^{-1}]			$C_{3\%}$
	$z=3$	$z=1$	$z=0$		$z=3$	$z=1$	$z=0$	
RPT/CLA	0.3	0.18	0.12	0.35	0.36	0.20	0.14	0.5
SPT	0.22	0.13	0.08	0.18	0.29	0.16	0.11	0.3
LIN	0.13	0.09	0.06	0.06	0.19	0.12	0.08	0.13

that $C^{\rm RPT,CLA}_{1\%}=0.35$, $C^{\rm SPT}_{1\%}=0.18$ and $C^{\rm LIN}_{1\%}=0.06$ well reproduce the 1% agreement limit of RPT/CLA, SPT and linear theory from figure 4, respectively. We plot equation (18) with these constant values as solid lines in figure 5 and also as vertical arrows in figure 4. Similarly we find that the corresponding 3% limits are given by $C^{\rm RPT,CLA}_{3\%}=0.5$, $C^{\rm SPT}_{3\%}=0.3$ and $C^{\rm LIN}_{3\%}=0.13$ for the three theoretical predictions (dashed lines in figure 5).

The convergence regimes of our criteria [equation (18)] are narrower than those previously proposed. Note, however, that the criteria (18) with the above constant values reasonably describe the valid range of analytic models even at higher redshifts ($z=7$ and 15). One of the possible sources of the difference between our criterion and the previous ones is that they use simulations with smaller box sizes to achieve better resolution, which enhances a systematic error due to the finiteness of box size. More details are discussed in the appendix.

6. Implications for the Phases of BAOs

6.1. Extraction of the phases of BAOs from the nonlinear power spectra

So far we have focused on the amplitudes of the matter power spectra, but the phase information of BAOs is also important. This is imprinted mainly in the leading term which is the product of the linear power spectrum and the propagator in RPT and CLA [see equation (2)]. Since the other contributions, the mode-coupling terms, are fairly smooth functions of wavenumber, the phase information of BAOs is almost erased by the convolution of the smoothed kernel and the propagator [1]. Therefore almost all of the BAO information comes from the zeroth-order term in RPT/CLA. We thus expect that the phase of BAOs predicted by N-body simulations and theories agree with each other for a wider range of wavenumbers compared to the amplitudes since the amplitudes are sensitive to higher-order corrections.

We test the convergence of the predicted phases of BAOs as follows. We first construct a smooth reference power spectrum using the spline technique developed by Percival et al. (2007) and Nishimichi et al. (2007). We adopt a basis spline (B-spline) fitting function as the reference spectrum, $P^{\rm B-spline}(k)$, with the break points at $k^{\rm break}_0=0.001h$Mpc^{-1} and $k^{\rm break}_j=(0.05j-0.025)h$Mpc^{-1} where j is a positive integer. The data points to be fitted are set at k_i of

[1] The mode-coupling term has very small wiggly feature which comes from BAOs. This leads to a sub-percent level shift of the positions of "nodes". See Crocce & Scoccimarro (2008) for more details.

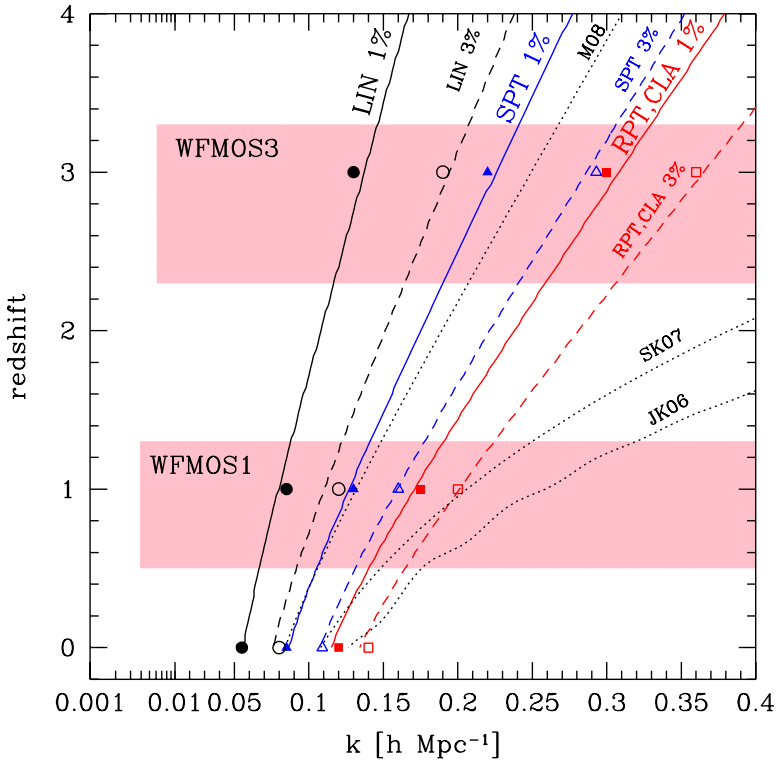

Fig. 5. Upper limit of reliable wavenumbers, $k^{\rm lim}_{1\%}$ and $k^{\rm lim}_{3\%}$, described in the text. Symbols show the values read from figure 4. *circles*: linear theory, *triangles*: SPT, *squares*: RPT/CLA. Filled symbols correspond to $k^{\rm lim}_{1\%}$, while open ones represent $k^{\rm lim}_{3\%}$. The three solid lines plot equation (18): $k^{\rm lim}_{1\%}$ for linear theory ($C = 0.06$), SPT ($C = 0.18$) and RPT/CLA ($C = 0.35$) from left to right, and the dashed lines are corresponding $k^{\rm lim}_{3\%}$ ($C = 0.13$, 0.3 and 0.5, respectively). We also show the nonlinear wavenumbers proposed by Jeong & Komatsu (2006), Sefusatti & Komatsu (2007) and Matsubara (2008) as dotted lines with JK06, SK07 and M08. The two shaded regions show the redshift range planed by WFMOS survey (with minimum wavenumbers, $2\pi/V^{1/3}$. Here V is the survey volume.).

equation (4) with a bin width of $\Delta k = 0.005h{\rm Mpc}^{-1}$ for both the N-body simulations results and the theoretical predictions. We use the N-body power spectrum, $\hat{P}^{N-{\rm body}}_{\rm corrected}(k,z)$, in which the effect of finite volume is corrected using perturbation theory. We assign equal weights to all data points. A smooth reference spectrum is computed for the average of the simulations and the theoretical models.

We then divide the model and N-body power spectra by their respective smooth reference power spectra, $P^{\rm B-spline}(k)$, described above, which are shown in figure 6. The symbols and lines have the same meanings as in figure 4. Among the three nonlinear models, RPT and CLA lie almost on top of each other, and they are indistinguishable. These two models show better agreement with N-body simulations than SPT, whose predicted strong damping of oscillations incorrectly leads to a phase reversal ($k \gtrsim 0.25h{\rm Mpc}^{-1}$ at $z = 1$, $k \gtrsim 0.16h{\rm Mpc}^{-1}$ at $z = 0$). Compared with the vertical arrows which represent the values of $k^{\rm lim}_{1\%}$ determined by the amplitudes of the power spectra, the convergence regimes of BAO phases predicted by analytic

models and N-body simulations are quite a bit wider. We thus conclude that the phases of BAOs are potentially more robust and more useful in the actual analysis of BAO surveys.

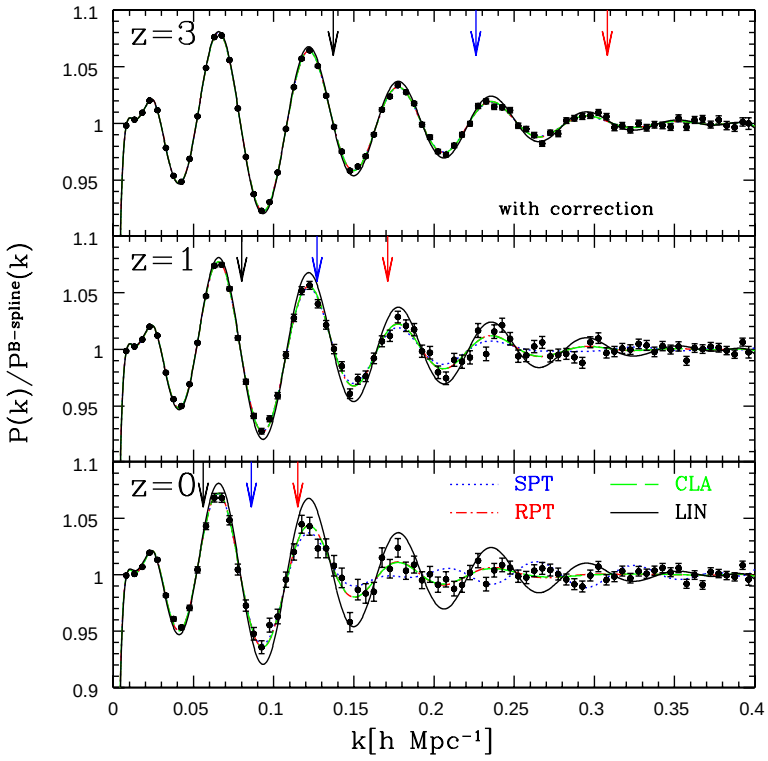

Fig. 6. Power spectra divided by their B-spline fits described in the text. Symbols, lines and vertical arrows are analogous of those in figure 4.

6.2. Recovery of the BAO scale from WFMOS survey

With our criteria for trustable ranges of simulations and analytic models, we are able to discuss future cosmological constraints using BAOs. A number of simulation papers attempted to present parameter forecasting of the dark energy equation of state parameter, $w_{\rm DE} \equiv p_{\rm DE}/\rho_{\rm DE}$, using BAOs as a standard ruler (i.e., Meiksin, White & Peacock 1999; Springel et al. 2005; Angulo et al. 2005, 2008; Eisenstein, Seo & White 2007; Eisenstein et al. 2007; Seo & Eisenstein 2003, 2005; Seo et al. 2008; Smith, Scoccimarro & Sheth 2007, 2008; White 2005; Huff et al. 2007; Jeong & Komatsu 2006, 2008). We follow a similar procedure, taking into account the reliable range of wavenumbers in the prediction of the BAO scale.

We consider the Wide-Field Multi-Object Spectrograph (c.f., Bassett, Nichol & Eisenstein 2005, WFMOS) as a specific example in the present analysis. We construct the template power ratio, $P/P^{\rm B-spline}(k)$, using RPT and linear theory as described above. We create mock power spectra by adding Gaussian random errors (Feldman, Kaiser & Peacock 1994):

$$\Delta\left(\frac{P(k)}{P^{\rm B-spline}(k)}\right) \approx \frac{\Delta P(k)}{P(k)} = \sqrt{\frac{2}{N^{\rm modes}}}\left[1+\frac{1}{n_g P(k)}\right]. \tag{19}$$

We neglect the errors arising from the construction process of $P^{\rm B-spline}(k)$. In the above expression, $N^{\rm modes}$ is the number of modes in the wavenumber bin $k \sim k + \Delta k$:

$$N^{\rm modes} = \frac{k^2 \Delta k V}{2\pi^2}, \tag{20}$$

where V denotes the survey volume, and n_g in equation (19) is the mean number density of galaxies. We set Δk to be very small ($0.001h{\rm Mpc}^{-1}$) so as not to affect the results and use the nonlinear matter power spectrum of Smith et al. (2003) for the calculation of the shot noise contribution, $[n_g P(k)]^{-1}$, just for simplicity.

We fit these mock data to the corresponding theoretical template $P/P^{\rm B-spline}(\alpha k)$ with a single free parameter α, the ratio of the true distance scale to the assumed one. The response of the *observed* power spectrum, $P_{\rm obs}(k,z)$, to the parameter α can be written as (e.g., Jeong & Komatsu 2008)

$$P_{\rm obs}(k,z) = \alpha^{-3} P_{\rm true}(\alpha k, z); \qquad \alpha \equiv \frac{D_{\rm V,true}}{D_{\rm V,fid}}, \tag{21}$$

where $P_{\rm true}(k,z)$ is the true power spectrum and $D_{\rm V}(z) \propto [D_{\rm A}^2(z)/H(z)]^{1/3}$, where $D_A(z)$ is the angular diameter distance (Eisenstein et al. 2005). $D_{\rm V,true}(z)$ represents the true distance, while $D_{\rm V,fid}(z)$ is calculated assuming the fiducial cosmology. In fitting the templates, we fix the value of the minimum wavenumber, $k_{\rm min}$, to be $0.02h{\rm Mpc}^{-1}$, while the value of the maximum wavenumber, $k_{\rm max}$, is varied. The assumed parameters for the $z \sim 1$ ($z \sim 3$) WFMOS survey are taken from Glazebrook et al. (2005): $V = 4h^{-3}{\rm Gpc}^3$ ($1h^{-3}{\rm Gpc}^3$) for the volume, $n_g = 5 \times 10^{-4} h^3 {\rm Mpc}^{-3}$ ($5 \times 10^{-4} h^3 {\rm Mpc}^{-3}$) for the galaxy number density, and $b = 2.0$ (3.5) for the linear bias parameter.

We employ a Markov chain Monte Carlo fitting routine to determine the uncertainty in the scale shift, σ_α, adopting RPT for the fiducial spectrum. We plan to do a similar fitting with more free parameters in future work. Figure 7 show the uncertainty in the scale shift, σ_α, as a function of $k_{\rm max}$ (solid lines). We also plot the results when we do not include shot noise and nonlinear degradation of BAOs (linear template) by the dashed lines. As a reference, vertical solid and dashed arrows indicate $k_{1\%}^{\rm lim}$ for RPT and linear theory, respectively. The difference of solid and dashed lines correspond to the impact of nonlinearity and shot noise, i.e., the information of phase of BAOs is lost due to these effects. The resulting error of α is 0.7(1.0)% at $z = 1(3)$ when we adopt $k_{1\%}^{\rm lim}$ of RPT/CLA as $k_{\rm max}$. These values are slightly improved and become 0.6(1.0)% if we increase $k_{\rm max}$ to $0.4h{\rm Mpc}^{-1}$. We can put a strong constraint on α even if we do not include the modes at $k > k_{1\%}^{\rm lim}$ of RPT in the analysis. In reality, however, we need to take account of *galaxy* clustering in *redshift space* in addition to what we did in the current paper, which will be presented in future work.

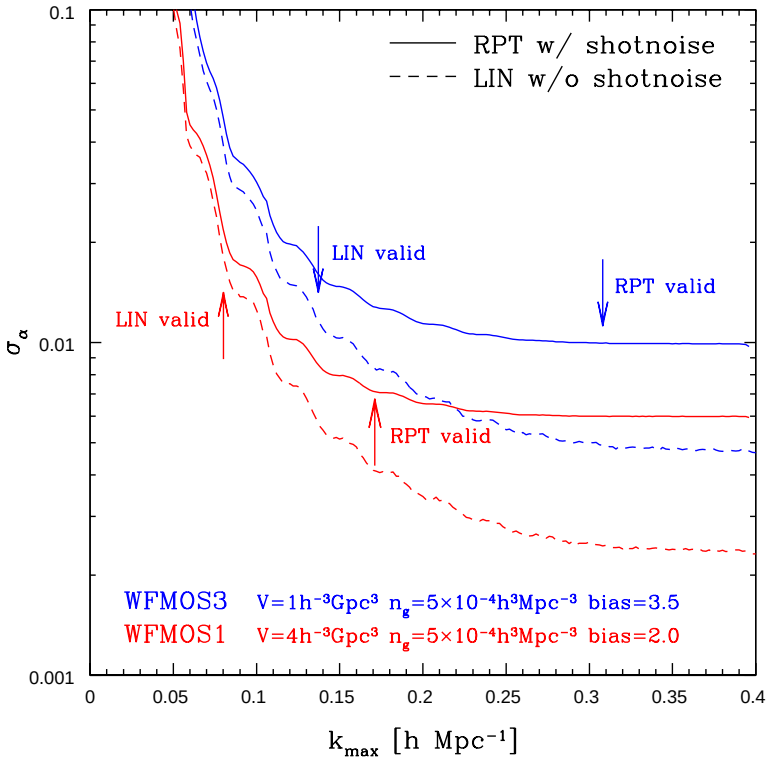

Fig. 7. Estimated constraints on the scale shift parameter, α, for both the wide ($z \sim 1$, red) and the deep ($z \sim 3$, blue) components of the proposed WFMOS survey. The solid lines show the results when we use RPT as the template spectrum, while the dashed ones correspond to an ideal case of no shot noise and no nonlinear degradation of BAOs (using the linear theory template). We fix the minimum wavenumber to be used in the fitting, $k_{\rm min} = 0.02h{\rm Mpc}^{-1}$, and the results are plotted as a function of the maximum wavenumber. The assumed survey parameters are written in the figure.

7. Summary

We have carried out a systematic comparison of power spectra calculated from N-body simulations and various theoretical models. We correct for the effect of finite volume of N-body simulations using the perturbation-theory-based methodology developed in Takahashi et al. (2008).

We find that our simulations agree with all the theoretical models used in the present paper at large length scales ($k \lesssim 0.1h{\rm Mpc}^{-1}$). At smaller length scales where nonlinearity is mild, our simulations, RPT (Crocce & Scoccimarro 2006a, b, 2008) and CLA (Taruya & Hiramatsu 2008) agree with 1% and 3% accuracies up to $k_{1\%}^{\rm lim}$ and $k_{3\%}^{\rm lim}$ as presented in figure 5. These convergence regimes depend on the redshift and can be explained by a simple empirical formula of equation (18). We also showed that the phase information of BAOs extracted from power spectra using B-spline fitting is more robust than the amplitudes: predicted phases of nonlinear theories and N-body simulations agree well in a wider range of wavenumbers than the amplitudes of the power spectrum.

The currently achieved accuracies of both theoretical predictions and simulations are sufficient to interpret the data from future surveys like WFMOS: one can put a tight constraint on the BAO scale ($\sigma_\alpha \lesssim 1\%$) using modes within our convergence regimes. There is the potential to extract more than simply the BAO scale from the power spectrum, such as the sum of the neutrino masses, if one is able to exploit smaller scale information (e.g., Saito, Takada & Taruya 2008). To this end, it is important to consider higher-order corrections (i.e., 2-loop terms) on the theory end and higher resolution simulations. It is also important to investigate the accuracy of the velocity field in N-body simulations to model accurately in redshift space. These are future investigations and a study in redshift space is now in progress.

We also checked the convergence of the matter power spectrum in N-body simulations changing the initial conditions, N-body solvers, and box sizes. Among these we showed that N-body simulations with small box sizes ($\lesssim 500h^{-1}$Mpc) suffer from systematic enhancements of the matter power spectra at BAO scales (e.g., Springel et al. 2005; Seo & Eisenstein 2005; Jeong & Komatsu 2006).

We thank S. Habib, R. Scoccimarro, M. Takada and E. Reese for useful suggestions and comments on the present paper. This work is supported in part by Japan Society for Promotion of Science (JSPS) Core-to-Core Program "International Research Network for Dark Energy". T.N., A.S., K.Yahata and I.K. acknowledge the support from the JSPS Research Fellows. S.S. is supported by Global COE Program "the Physical Sciences Frontier", MEXT, Japan. Y.P.J. is supported by NSFC (10533030, 10821302, 10878001), by the Knowledge Innovation Program of CAS (No. KJCX2-YW-T05), and by 973 Program (No.2007CB815402). This work is supported by Grants-in-Aid for Scientific Research from the JSPS (Nos. 18740132, 18654047, 19840008) and by Grant-in-Aid for Scientific Research on Priority Areas No. 467 "Probing the Dark Energy through an Extremely Wide & Deep Survey with Subaru Telescope".

References

Angulo, R., et al., 2005, MNRAS, 362, 25
Angulo, R. Baugh, C. M., Frenk, C. S., & Lacey, C. G., 2008, MNRAS, 383, 755
Baertschiger, T., Joyce, M., & Sylos Labini, F., 2002, ApJ, 581, 63
Bassett, B. A., Nichol, R. C., & Eisenstein, D. J., 2005, the WFMOS Feasibility Study Dark Energy Team, arXiv:astro-ph/0510272
Bernardeau, F., Colombi, S., Gaztañaga, E., and Scoccimarro, R., 2002, Phys. Rep., 367, 1
Bode, P., & Ostriker, J. P., 2003, ApJS, 145, 1
Crocce, M., & Scoccimarro, R., 2006a, Phys. Rev. D, 73, 063519
Crocce, M., & Scoccimarro, R., 2006b, Phys. Rev. D, 73, 063520
Crocce, M., Pueblas, S., & Scoccimarro, R., 2006, MNRAS, 373, 369
Crocce, M., & Scoccimarro, R., 2008, Phys. Rev. D, 77, 023533

Eisenstein, D. J., & Hu, W., 1998, ApJ, 496, 605
Eisenstein, D. J., et al., 2005, ApJ, 633, 560
Eisenstein, D. J., Seo, H. J., & White, M., 2007, ApJ, 664, 660
Eisenstein, D. J., Seo, H. J., Sirko, E., & Spergel, D., 2007, ApJ, 664, 675
Feldman, H. A., Kaiser, N., & Peacock, J.A., 1994, ApJ, 426, 23
Glazebrook, K., Eisenstein, D., Dey, A., Nichol, B., & The WFMOS Feasibility Study Dark Energy Team., 2005, ArXiv Astrophysics e-prints, astro-ph/0507457
Hamana, T., Yoshida, N., & Suto, Y., 2002, ApJ, 568, 455
Hockney, R. W, & Eastwood, J. W., 1981, Computer Simulations Using Particles (New York: McGraw-Hill)
Huff, E., Schulz, A. E., White, M., Schlegel, D. J., & Warren, M. S., 2007, APh, 2007, 26, 351
Jain, B., & Bertschinger, E., 1994, ApJ, 431, 495
Jeong, D., & Komatsu, E., 2006, ApJ, 651, 619
Jeong, D., & Komatsu, E., 2008, arXiv:0805.2632, accepted by ApJ
Jing, Y. P., & Suto, Y., 1998, ApJ, 494, 5
Jing, Y. P., & Suto, Y., 2002, ApJ, 574, 538
Jing, Y. P., 2005, ApJ, 620, 559
Joyce, M., Marcos, B., 2007, Phys. Rev. D, 2007, 75, 063516
Joyce, M., Marcos, B., 2007, Phys. Rev. D, 2007, 76, 103505
Joyce, M., Marcos, B.,& Baertschiger, T., 2008, arXiv:0805.1357
Lewis, A., Challinor, A., & Lasenby, A., 2000, ApJ, 538, 473
Meiksin, A., White, M., & Peacock, J. A., 1999, MNRAS, 304, 851
Makino, N., Sasaki, M., & Suto, Y., 1992, Phys. Rev. D, 46, 585
Marcos, B., et al., 2006, Phys. Rev. D, 2006, 73, 103507
Matarrese, S., & Pietroni, M., 2008, MPLA, 2008, 23, 25
Matarrese, S., & Pietroni, M., 2007, JCAP, 06, 026
Matsubara, T., 2008, Phys. Rev. D, 77, 063530
McDonald, P., 2007, Phys. Rev. D, 75, 043514
Meiksin, A., White, M., & Peacock, J. A., 1999, MNRAS, 304, 851
Melott, A. L, Shandarin, S. F., Splinter, R. J., & Suto, Y., 1997, ApJ, 479, 79
Nishimichi, T., et al., 2007, PASJ, 59, 1049
Percival. W., et al., 2007, ApJ, 657, 51
Romeo, A. B., Agertz, O., Moore, B., & Stadel, J., 2008, arXiv:0804.0294, ApJ, in press
Saito, S., Takada, M., & Taruya, A., 2008, Phys. Rev. Lett., 100, 191301
Scoccimarro, R., & Frieman, J. A., 1996, ApJ, 473, 620
Sefusatti, E., & Komatsu, E., 2007, Phys. Rev. D, 76, 083004
Seo, H. J., & Eisenstein, D. J., 2003, ApJ, 598, 720
Seo, H. J., & Eisenstein, D. J., 2003, ApJ, 633, 575
Seo, H. J., Siegel, E. R., Eisenstein, D. J., and White, M., 2008, arXiv:0805.0117, accepted by ApJ
Seto, N., 1999, ApJ, 523, 24
Smith, R. E., et al., 2003, MNRAS, 341, 1311

Smith, R. E., Scoccimarro, R., & Sheth, R. K., 2007, Phys. Rev. D, 75, 063512
Smith, R. E., Scoccimarro, R., & Sheth, R. K., 2008, Phys. Rev. D, 77, 043525
Spergel, D. N., et al., 2007, ApJS, 170, 377
Splinter, R. J., Melott, A. L, Shandarin, S. F., & Suto, Y., 1998, ApJ, 497, 38
Springel, V., 2005, MNRAS, 364, 1105
Springel, V., et al., 2005, Nature, 435, 629
Takahashi, R., et al., 2008, MNRAS, 389, 1675
Taruya, A., & Hiramatsu, T., 2008, ApJ, 674, 617
Valageas, P., 2007, A&A, 465, 725
White, M., 2005, APh, 24, 334
Zel'dovich, Y. B., 1970, A&A, 5, 84

Appendix 1. Convergence check of different *N*-body codes and dependence on simulation parameters

A.1.1. Initial Condition Generator

We test two methods for generating cosmological initial conditions. One is the Zel'dovich approximation (Zel'dovich 1970; hereafter ZA) commonly used for cosmological simulations, and the other is second-order Lagrangian perturbation theory (2LPT; e.g., Crocce, Pueblas & Scoccimarro 2006). Starting from the same linear density field, $\delta^{\rm L}_{{\bf k},n}$, we generate two initial conditions at $z_{\rm ini} = 31$ from N-body runs using ZA and 2LPT. Then we compare the power spectra evolved with `Gadget2`.

Figure 8 shows the ratio of the two matter power spectra from simulations at various output redshifts. The overall trend that $P^{\rm ZA}(k)$ has smaller amplitudes at all scales than $P^{\rm 2LPT}(k)$ is consistent with the result of Crocce, Pueblas & Scoccimarro 2006. This is because the higher-order terms in ZA do not necessarily correspond to the growing solutions. The plot indicates that differences in the initial conditions affect the power spectrum at the few percent level. We confirmed that this difference between 2LPT and ZA reduces to subpercent when we increase the starting redshift to $z_{\rm ini} = 127$. However, we need a very large number of mesh points in the calculation of the PM force to avoid large errors introduced by the tree force that arise when the density field is nearly uniform. This is very time consuming. Thus we need 2LPT initial condition for the purpose of present analysis if we start the simulations at $z_{\rm ini} = 31$. We also confirm that our 2LPT result is not affected when we change the starting redshift to $z_{\rm ini} = 63$ or $z_{\rm ini} = 127$.

A.1.2. Comparison using different N-body solvers

Next we compare three different N-body solvers; a Tree-Particle-Mesh (Tree-PM) solver `Gadget2` (Springel 2005), another Tree-PM code `TPM` of Bode & Ostriker (2003), and a Particle-Particle-Particle-Mesh ($\rm P^3M$) code developed in Jing & Suto (1998, 2002; hereafter `JS02`). We use identical initial conditions as that of one of our fiducial runs, 512^3 particles in a box

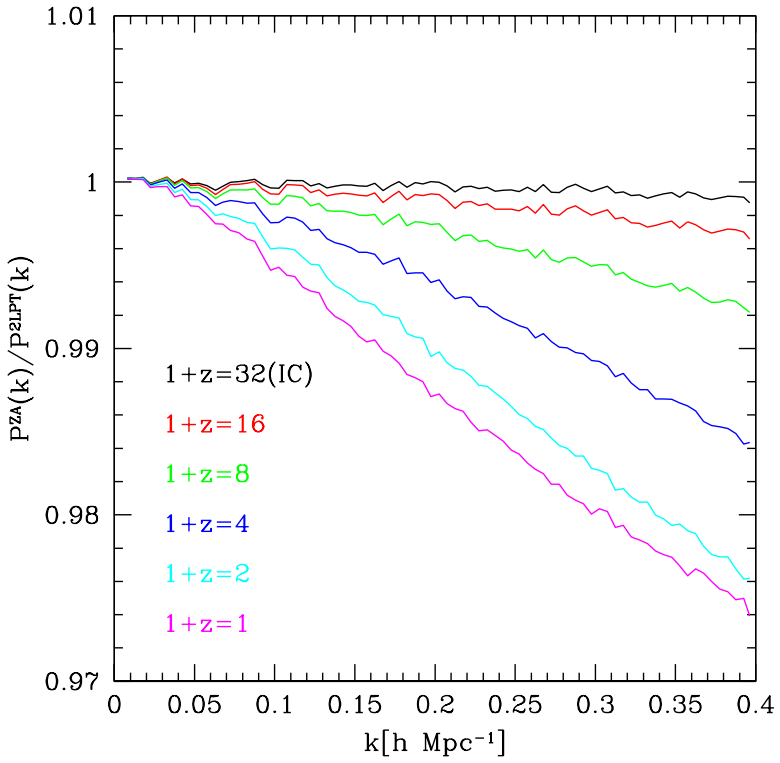

Fig. 8. We plot the evolution of the power spectrum from two simulations using a ZA initial condition and a 2LPT. To see the difference clearly, we show the ratio $P^{\rm ZA}/P^{\rm 2LPT}$ at a number of output times.

of $1000h^{-1}$Mpc. We stop the simulations at $z = 3$. In addition to the Tree-PM and P^{3}M calculations, we also run simulations using only the PM part of the three codes. We measure the power spectra for the simulation output at $z = 3$ and correct for the effect of finite volume (see section 4 above) so that the comparison is clearer.

Figure 9 shows the relative difference from the RPT prediction, $[\hat{P}^{N-{\rm body}}_{\rm corrected}(k) - P^{\rm RPT}(k)]/P^{\rm nw}(k)$. The upper panel shows the results when we include the short-range forces (i.e., tree or particle-particle force). The result of `TPM`, `JS02` and `Gadget2` are shown by dotted, dashed and solid lines with errorbars, respectively. We omit the errorbars for `TPM` and `JS02` as these are almost the same as for `Gadget2`, which is given by equation (13). The overall behaviours for the three codes are very consistent, and the difference is important ($\gtrsim 1\%$) only at smaller scale than $k^{\rm lim}_{1\%}$ of RPT/CLA shown by the vertical arrow. In the bottom panel we plot the results of the three codes when we use only PM forces. The degree of dispersion among the three is larger than that in the upper panel, and is $\sim 3\%$ at $k^{\rm lim}_{1\%}$ of RPT/CLA. The short-range force is helpful to increase the accuracy at this level at this scale. We conclude that our main result is not affected so much by the choice of particular N-body solver when we turn on the short-range force.

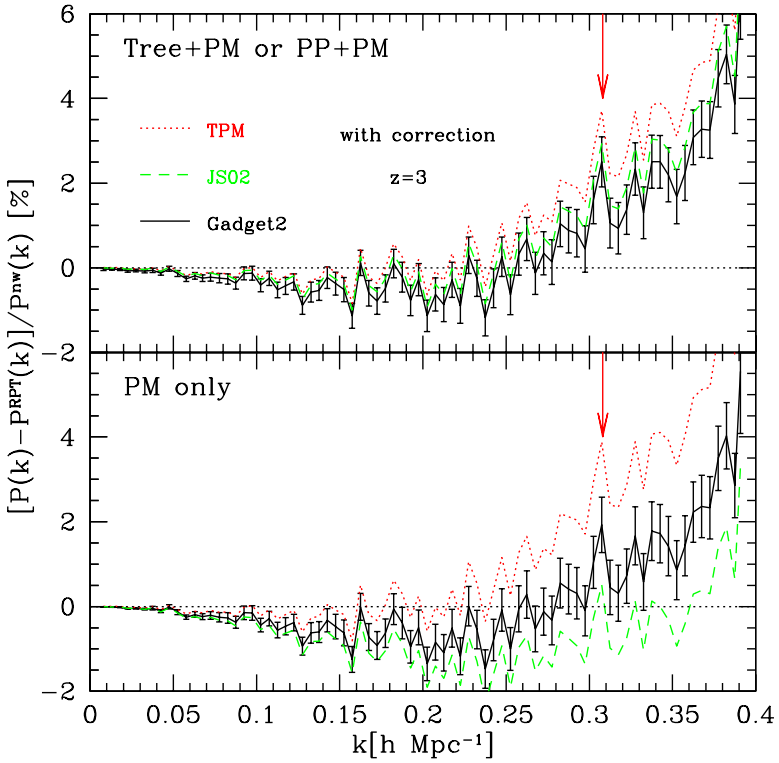

Fig. 9. A comparison of different N-body simulation codes. We plot $[\hat{P}^{N-\mathrm{body}}_{\mathrm{corrected}}(k) - P^{\mathrm{RPT}}(k)]/P^{\mathrm{nw}}(k)$ at $z=3$. Different line types correspond to `TPM` (dotted), `JS02` (dashed) and `Gadget2` (solid), respectively. The vertical arrows show the limit wavenumber $k^{\mathrm{lim}}_{1\%}$ for RPT/CLA. The errorbars are given by equation (13) for `Gadget2`. *Upper*: Results of Tree-PM and PP-PM calculations. *Lower*: Results of PM only calculations.

A.1.3. Effects of finite box size and resolution

The finite box size introduces an additional variance in the power spectrum as shown in Takahashi et al. (2008) and this work. It is possible that this finiteness affects not only the variance but also the mean value. The resolution of simulations may also affect the results. We thus investigate the box size/resolution dependence of the power spectra from N-body simulations.

In order to increase the spatial resolution, we run simulations varying the box size [1000 (4 realizations; fiducial), 500 (7 realizations) and $250h^{-1}$Mpc (9 realizations)] but keeping the number of particles to be the same as our fiducial runs (512^3) to check the convergence. For this test, we use outputs at $z=3$. The results are shown in figure 10. Symbols correspond to $L_{\mathrm{box}}=1000h^{-1}$Mpc (circle), $500h^{-1}$Mpc (triangle) and $250h^{-1}$Mpc (square). We adopt the bin width $\Delta k=0.01h\mathrm{Mpc}^{-1}$ in this section for clarity. We also calculate the RPT predictions with the effect of finite box size by introducing a cut-off scale ($k_{\mathrm{box}}\equiv 2\pi/L_{\mathrm{box}}$) in the integration, which are shown in the left panel. The solid line is the normal RPT result (without cut-off), and the other lines take account of the effect of finite box size (short-dashed: $1000h^{-1}$Mpc, long-dashed: $500h^{-1}$Mpc and dot-dashed: $250h^{-1}$Mpc). Note that we show only the results

without cutoff in the text. In the right panel, we plot a comparison with the SPT prediction (no cut-off) to show the dependence on the box size of the valid ranges of SPT.

In the left panel, one may notice the difference of theoretical lines at large wavenumbers. This reflects the finiteness of the box: short-dashed line ($L_{\rm box} = 1000h^{-1}$ Mpc case) deviates from solid line (infinite volume case) only at $k > 0.3h$ Mpc $^{-1}$ and is very small ($\sim 0.5\%$ at $k = 0.4h$ Mpc $^{-1}$), whereas long-dashed and dash-dotted ones ($L_{\rm box} = 500$ and $250h^{-1}$ Mpc cases) diverge at smaller wavenumbers and to a greater degree ($\sim 1.5\%$ and $\sim 3\%$ at $k = 0.4h$ Mpc $^{-1}$, respectively). Although the results of N-body simulations with smaller box sizes have larger variances due to smaller total volumes than the fiducial runs, box size dependence appears at small scales. The runs with smaller box size tend to have larger amplitudes, which is consistent with RPT predictions with cutoff scales. We thus conclude that the results of simulations also suffer from a systematic effect due to finite box size, and adopt $L_{\rm box} = 1000h^{-1}$Mpc for our fiducial model, where the effect is $\lesssim 0.5\%$.

Next, the convergence regime of SPT seems wider if one believes the results of the smaller box size runs in the right panel. We consider these wider valid ranges are just coincidences due to the systematic effects in the simulations with smaller box sizes and should not be trusted. One should keep this in mind when one uses the results of simulations with small box size. Even the Millennium simulation (Springel et al. 2005) has only $500h^{-1}$Mpc on each side, although it has many more particles (2160^3) than ours and thus the spacial resolution is better. This box size introduces $\gtrsim 1\%$ systematics at $k \gtrsim 0.35h$Mpc^{-1} according to our figure 10. Part of the disagreement in the valid range of SPT between our results and that of Jeong & Komatsu (2006) may be due to this effect, as they use $L_{\rm box} = 512$, 256, 128 and $64h^{-1}$Mpc.

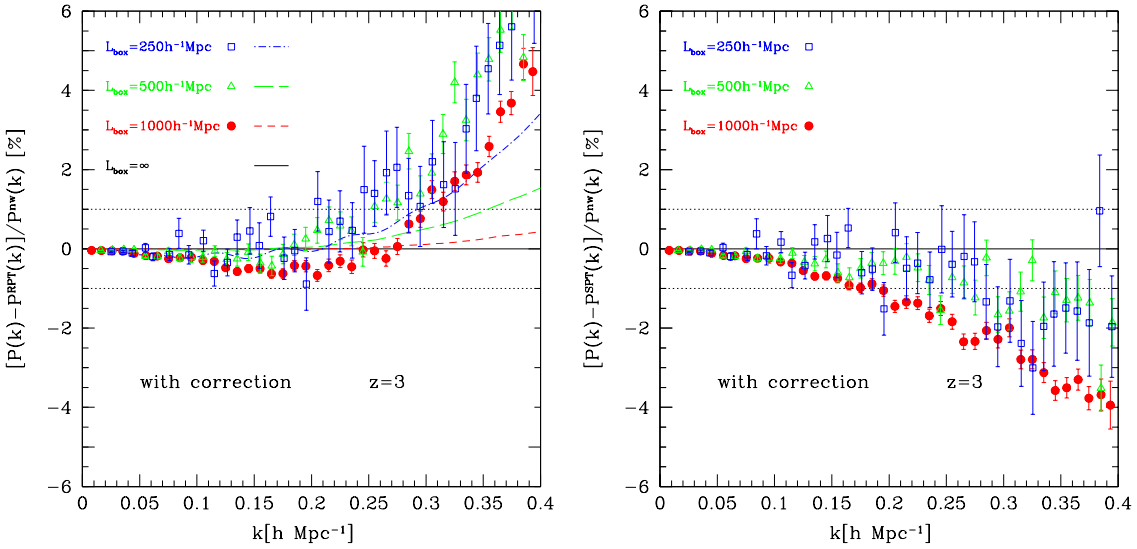

Fig. 10. We compare results of N-body simulations for different box sizes at $z = 3$. *circle*: $1000h^{-1}$Mpc, *triangle*: $500h^{-1}$Mpc, *square*: $250h^{-1}$Mpc. *Left*: comparison with the RPT prediction (dotted line). We also plot predictions of RPT taking account of the finiteness of the volume by introducing a cut off scale: *solid*: *short-dashed*: $1000h^{-1}$Mpc (dashed), $500h^{-1}$Mpc (long-dashed) and $250h^{-1}$Mpc (dot-dashed). *Right*: comparison with the SPT prediction, in which we do not take account of the finiteness effect.